ELSEVIER

Physica C 241 (1995) 198–207

PHYSICA C

Low-temperature melt growth of $YBa_2Cu_3O_{7-x}$/silver composites in partial vacuum

Nae-Lih Wu, H.H. Zern, Chi-Liang Chen

Chemical Engineering Department, National Taiwan University, Taipei, Taiwan

Received 16 September 1994; revised manuscript 19 October 1994

Abstract

A new version of the $YBa_2Cu_3O_{7-x}$ (the 123 oxide) melt-growth (MG) process, which is carried out under greatly reduced oxygen pressures (in partial vacuum) at temperatures not higher than 950°C, is described. Some salient aspects of this process are demonstrated with examples of processing 123/Ag composites in bulk and 123-on-Ag tape forms under the conditions of $0.01 \leqslant P(O_2) \leqslant 10$ Torr and $920 \leqslant T \leqslant 950$°C. In addition to the 123 domain structure, Y_2BaCuO_5 inclusions and strong pinning typical of MG-123, the bulk composites thus synthesized contain uniformly dispersed Ag inclusions, which are effective in suppressing cracking within the 123 domains, while the 123-on-Ag tapes show *c*-axis preferential orientation of the 123 film normal to the Ag substrate, good oxide–substrate adhesion, and particularly negligible Ag melting. On the basis of microstructural observations, the mechanisms for the engulfment of Ag inclusions during solidification and for the enhancement in resistance to crack growth by the Ag inclusions are revealed.

1. Introduction

Supercurrent-carrying capability and mechanical stability are two of the major concerns for realizing practical applications of the high-T_c superconducting oxides. Significant progress in raising the critical current density (J_c) of polycrystalline $YBa_2Cu_3O_{7-x}$ (also known as the 123 compound) was achieved in several melt-growth (MG) processes, including MTG (melt textured growth [1]), QMG (quench and melt growth [2]), and MPMG (melt powder melt growth [3]) methods. In these processes, briefly, a bulk 123 oxide preform is first melted, either in atmospheric oxygen or in air, at temperatures above its incongruent melting point ($\sim$1020 and 1000°C in atmospheric oxygen and air, respectively), then resolidified via slow cooling, and finally oxygenated at lower temperatures. A 123 bulk thus prepared typically shows the domain structure in which each domain consists of platelet-like 123 grains aligned along their *a*–*b*-planes and Y_2BaCuO_5 (the 211 oxide) inclusions. Intra-domain J_cs in the range of, for example, 10^4–10^5 A/cm^2 at 77 K under a field up to 1 T have routinely been reported [1–5]. Cracks, resulting from the change in specific volume during tetragonal-to-orthorhombic phase transformation of 123, are, however, frequently presented within the oxide domains. They are not only detrimental to the transport of supercurrent but also facilitate fracturing.

Silver (Ag) has been combined with 123 oxide in many solid-state sintering processes to prepare composites, which exhibit superior superconducting and mechanical properties to the pure 123 [6–14]. It has been used either as a dispersed phase filling the voids within the solid-state sintered 123 bulk [6–10] or as the sheath or substrate material in the 123/Ag composite wire or tape [11–14]. In the bulk composite, Ag addition has been found to improve resistance to

0921-4534/95/$09.50
SSDI 0921-4534(94)02324-7

thermal shock and subcritical crack growth, while, in the tape or wire one, Ag provides mechanical support to the thin 123 filaments or films. Moreover, the high thermal conductivity of Ag facilitates dissipation of the heat generated by flux jumping, and its high electrical conductivity lowers the normal-state resistance. Both effects could enhance the critical current density. However, introduction of Ag into the MG processing methodology for preparing 123/Ag composites in various forms has been either unsuccessful or not attempted. Reduction in J_c due to introduction of Ag into current MG processes has been noted [15–17]. The attempt to process the wire or tape-type of 123/Ag composites by the current MG processes is almost impossible due to expected extensive melting of Ag at the conventional processing temperatures, which range from 1050 to 970°C; well above the melting point of Ag (curve a in Fig. 1) [18].

The incongruent melting, i.e., peritectic decomposition, of the 123 oxide can be summarized by the following reaction:

$$123_{(s)} \Leftrightarrow 211_{(s)} + \text{Ba–Cu–O}_{(l)} + xO_{2(g)} .$$

Accordingly, the melting point decreases with decreasing oxygen pressure. While there have been a few reports [19–22] on the melting-solidification processing of 123 in sub-atmospheric oxygen, the issue of Ag addition has not been addressed and no attempt has been made to lower the processing temperatures. We describe in this paper the melt-growth processing of 123/Ag composites under greatly reduced oxygen pressures at temperatures no higher than 950°C. The low-oxygen-pressure environment was achieved by partial vacuum; therefore, the process will be termed hereafter as the partial vacuum melt growth (PVMG), although, as discussed later, the results are applicable to an atmospheric setup with greatly diluted oxygen concentrations. Syntheses of 123/Ag composites in bulk and tape forms are demonstrated.

2. Experimental

The PVMG heat treatments were carried out in a horizontal tubular quartz reactor with flowing oxygen at sub-atmospheric pressures. The pressure was continuously monitored and controlled by varying the oxygen flow rate while maintaining a fixed pumping rate. At the end of each PVMG process, the oxygen pressure was raised to 1 atm, under which the treated sample was oxygenated at descending temperatures not higher than 700°C. For bulk samples, the 123 powder was synthesized by the solid-state reaction method conducted at 930°C for several ten hours, while the Ag powder was used as purchased (<300 mesh). The phase purity of the 123 powder was checked by XRD and T_c measurements. The 123 and 123/Ag bulk preforms were prepared by uni-axially compressing either pure 123 or 123+Ag mixture powders into pellets of 1 cm in diameter and 0.3 cm thick, which were pre-sintered at 900–930°C for 10 h prior to PVMG treatment.

The 123-on-Ag tape was prepared by a spraying pyrolysis method, which has previously been described in detail [14]. In brief, a solution containing nitrates of Y, Ba and Cu was sprayed onto a heated Ag substrate. After a certain amount of materials was deposited, the tape was calcined at 920°C. The deposition–calcination cycle was repeated until the 123 film thickness reached the desired value. The microstructures were characterized primarily by polarized microscopy, while the compositions were analyzed by X-ray diffractometry (XRD). Magnetization measurement, using SQUID, was employed for determining the superconducting properties of processed specimens.

3. Results

There have been several reports on the phase stability of 123 oxide under subatmospheric oxygen pressures [18,23–27]. In particular, for pure 123, good agreements were found among the data reported by Lindemer et al. [18], Idemoto and Fueki [25], and Kale [26]. We have conducted a few experiments in which 123 powders with or without addition of Ag were first heated at different temperatures under various oxygen pressures and then quenched. By analyzing the compositions in the quenched materials based on XRD, we found that the results were consistent with their reported data. The lines (b) through (d) appearing in Fig. 1 show the T–$P(O_2)$ characteristics of 123 stability. They are drawn and extrapolated, as indicated by the dashed

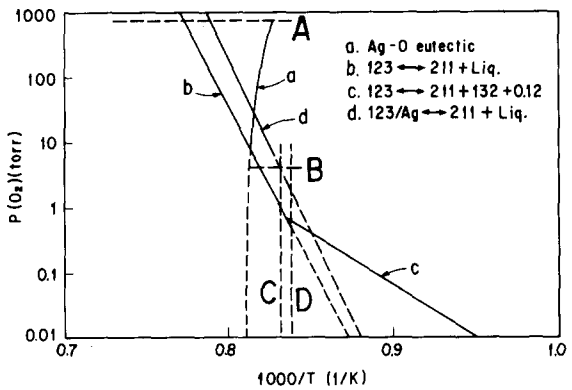

Fig. 1. Dependence of the 123 oxide stability on oxygen pressure, $P(O_2)$, and temperature, T, for pure 123 and 123/Ag. Also shown is the dependence of the melting of Ag. Lines (a)–(d) are drawn and extrapolated, as indicated by the dashed portions, based on the data in Refs. [18,27]. Compounds 211, 132 and 012 represent Y_2BaCuO_5, $YBa_3Cu_2O_x$, and $BaCu_2O_y$, respectively. The dashed lines #(A)–(D) indicate the four solidification routes employed in this work, with the first three (A–C) being for bulk samples and (D) for the tape.

portions of these lines, based on the data of Lindemer et al. [18,27]. When 123 is heated at a constant temperature under decreasing oxygen pressures, 123 exhibits two different decomposition behaviors (lines b and c in Fig. 1), depending on temperature. At temperatures higher than ~925°C, 123 incongruently melts to give the 211 solid and Ba–Cu–O liquid phases. Below this temperature, 123 first decomposes into three solid phases, including 211, $YBa_3Cu_2O_x$ (the 132 oxide), and $BaCu_2O_2$ (the 012 oxide), before it melts at lower oxygen pressures. The temperature, 925°C, at the transition between these two decomposition mechanisms is clearly the lower temperature limit of the PVMG process for pure 123. However, introduction of Ag causes the high-temperature solidus line to shift toward lower temperatures (line (d) in Fig. 1); therefore, a lower PVMG temperature limit may be obtained. Furthermore, it is clear from the figure that the PVMG process can be carried out by either varying temperature under a fixed oxygen pressure or vice versa.

Figs. 2a–2e compare the microstructures of the bulk 123/Ag composites and pure 123 prepared via three different solidification routes, of which the $P(O_2)$–T conditions are depicted by the dashed lines (A)–(C) in Fig. 1. They include route (A) cooling from 1100 to 920°C at a rate of 1 °C/h in 1 atm oxygen; a thermal history typical of the conventional MG processes; (B) cooling from 950 to 920°C at 2°C/h under a constant oxygen pressure of 4.2 Torr; and (C) raising the oxygen pressure from 0.01 to 10 Torr at a rate of 0.5 Torr/h at a constant temperature, 930°C. It was found that, by following route A, Ag (20% by weight) segregated into large lumps, which are preferentially trapped within the glass phase regions between 123 domains. During the experiments, a greater extent of melt-creep on crucible was noticed, and subsequent microstructure analyses show more glass materials remaining in the solidified bulk for the composite than for the pure 123. The increased amounts of glass materials, which are not superconducting, may account in part for the reduction in J_c for the MG-123/Ag reported in the literature [15–17]. Furthermore, within every 123 domain, many parallel cracks are clearly seen which are extending primarily along the low-angle grain boundaries of 123 and, in many occasions, throughout the entire domain.

Solidification via route B (PVMG with cooling from 950 to 920°C at 2°C/h with $P(O_2)=4.2$ Torr) produced not only the domain structures and 211 inclusions but also rather uniformly distributed Ag inclusions within 123 domains. The 123 domains have a size of 300–500 μm, while the intra-domain Ag inclusions are mostly 20–50 μm across. The total amounts of the Ag inclusions appearing on cross-section micrographs generally do not account fully for the originally added amount, which was 20% by weight. Ag deposit was found at the cold-end of the reactor, suggesting that some Ag evaporated during the PVMG treatment.

The notions that the PVMG process for pure 123 is limited at temperatures not lower than the transition temperature (~925°C) of the two different decomposition mechanisms of 123 and that this temperature limitation can be relieved to some extent by introducing Ag are evidenced by the following two examples. As shown in Fig. 2c, the pure 123 solidified via route C (raising $P(O_2)$ from 0.01 to 10 Torr at 930°C) is very porous. In particular, near the edge of the sample, where the temperature is presumably slightly lower than the set one, no domain structures were found but only randomly oriented 123 grains with grain sizes of a few tens μm, which are typical of the solid-state sintered 123 material. In contrast, the

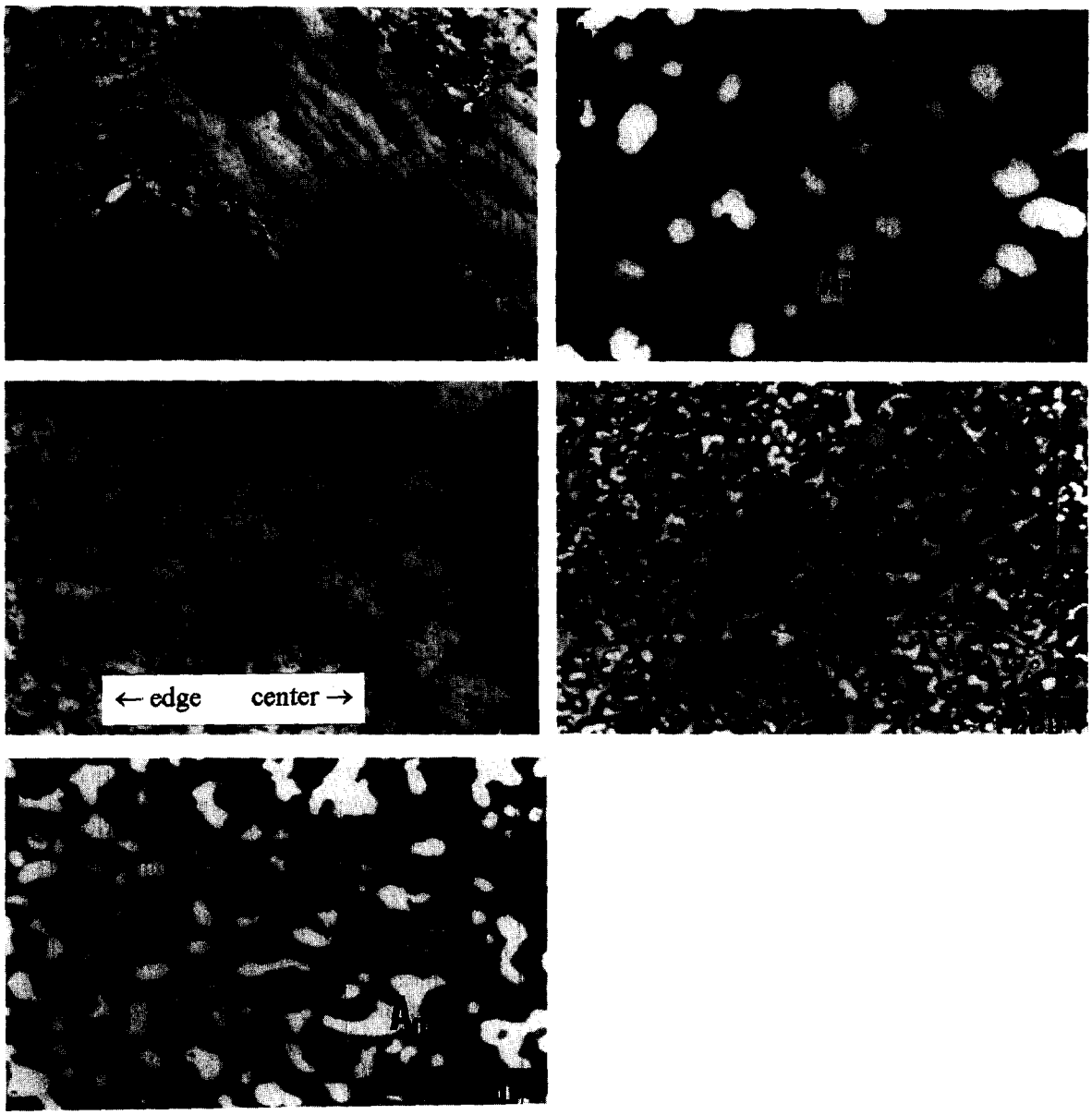

Fig. 2. Representative microstructures of the 123 and 123/Ag bulk samples subjected to different solidification processes: (a) 123/Ag (20 wt.%), cooling from 1100 to 920°C at 1°C/h with $P(O_2)=1$ atm; (b) 123/Ag (20 wt.%), cooling from 950 to 920°C at 2°C/h with $P(O_2)=4.2$ Torr; (c) pure 123, raising $P(O_2)$ from 0.01 to 10 Torr at 0.5 Torr/h with $T=930$°C; (d), (e) 123/Ag (50 wt.%), the same solidification conditions as in (c).

123/Ag composite (50 wt.% Ag) subjected to the same heat treatment exhibits a very dense domain structure and contains intra-domain Ag inclusions (Figs. 2d and 2e). The microstructural differences clearly suggest that there is a much greater extent of melting–resolidification reaction of 123 taking place in the composite sample than in the 123 one.

Compared with the route-B composite (Fig. 2b), the route-C one (Figs. 2d, 2e) has more voids, which result from Ag evaporation, because of a longer period of heat treatment in vacuum. Furthermore, comparisons among the route-A through C compos-

ites (Figs. 2a, 2b and 2d, 2e) also show that there are fewer and shorter cracks as the amounts of the intra-domain Ag inclusions increase. Evidences showing cracks being either pinned or bridged by the intra-domain Ag inclusions are abundant. This will be discussed in more detail later.

Under a field of 50 G, as characterized by DC magnetization measurements, the VMG-123/Ag bulk samples typically exhibit a T_c of ~90 K and a saturation of the field-cooled magnetization curve at ~80 K with more than 90% of the applied field being trapped (Fig. 3a). While the samples give different sizes of magnetization-hysteresis loops due to varied 123 domain sizes, the critical current densities calculated based on the Bean model [21] and assuming current loop only within oxide domain, are in the range of, for example, $1.0\text{–}5.0\times10^4$ A/cm^2 at 77 K under a field of 0.5 T (Fig. 3b), which are similar to the ones reported in the literature for pure MG-123.

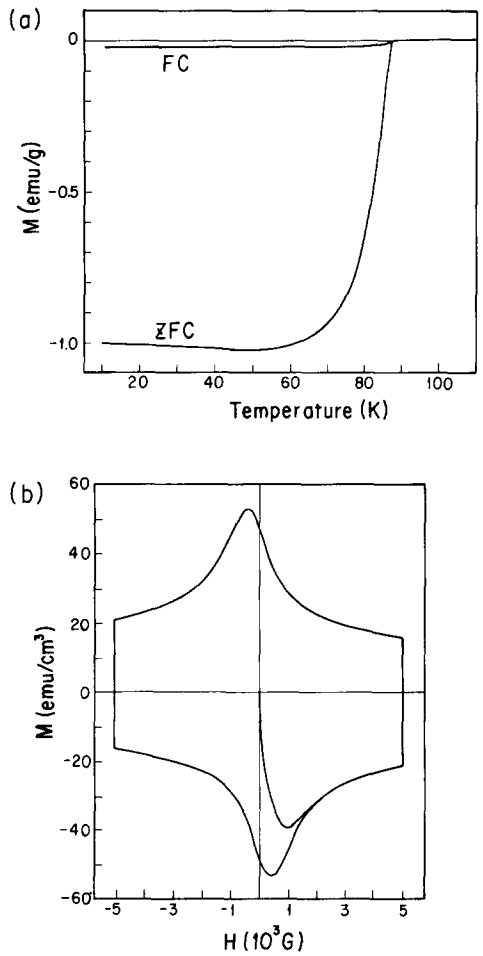

Fig. 3. Representative superconducting properties of bulk VMG-123/Ag composites. Shown are (a) the field-cooled (FC) and zero-field-cooled (ZFC) magnetization curves under 50 G; and (b) the magnetization-hysteresis loop at 77 K.

Syntheses of 123-on-Ag tapes have been aimed at temperatures not higher than 930°C in order to minimize Ag melting and loss via evaporation. Figs. 4a–4c show the morphologies of an Ag-supported 123 film (starting thickness = ~7μm) before (Fig. 4a) and after (Figs. 4b and 4c) being subjected to solidification at 920°C under increasing $P(O_2)$ from 0.01 to 10 Torr at a rate of 2 Torr/h (route D shown in Fig. 1). The starting 123 film (Fig. 4a) is composed of loosely packed 123 platelets that are ~5 μm across. After the PVMG process, the 123 film exhibits the domain structure which consists of dense 123 domains with a size ranging from ~100 μm to ~1 mm. The surfaces of the 123 domains are, in most cases, heavily faceted, and some of them are covered with incompletely solidified materials. Bare Ag is observed along some domain boundaries, arising due to an increase in local density within the oxide domains.

The processed tapes exhibit a good oxide/Ag interfacial bonding, as evidenced by the fact that the oxide film does not peel off even after several cycles of severe bending. XRD indicates that the PVMG-123 film has a texture of *c*-axis preferential orientation normal to the Ag substrate (Fig. 4d), a result similar to that found by Feenstra et al. [29] for a completely different process in this T–$P(O_2)$ range. The transport J_cs, measured by the four-probe method with the 1 μV/cm standard over a film length of 2 cm, are ~3000 and 1500 A/cm^2 at 40 and 77 K, respectively, under self-field. They are more than one order of magnitude lower than the intra-domain ones. The low transport J_c suggests poor linkage among 123 domains, which can partly be attributed to the film discontinuity observed at domain boundaries. Increasing the density and/or thickness of the starting 123 film may alleviate this problem.

The presence of the domain structure in thus synthesized PVMG-123 films suggests that the oxide film has indeed gone through the melting–resolidification cycle. However, according to Fig. 1, the processing temperature (920°C) in this case is below the PVMG temperature limit for pure 123 but above that for the

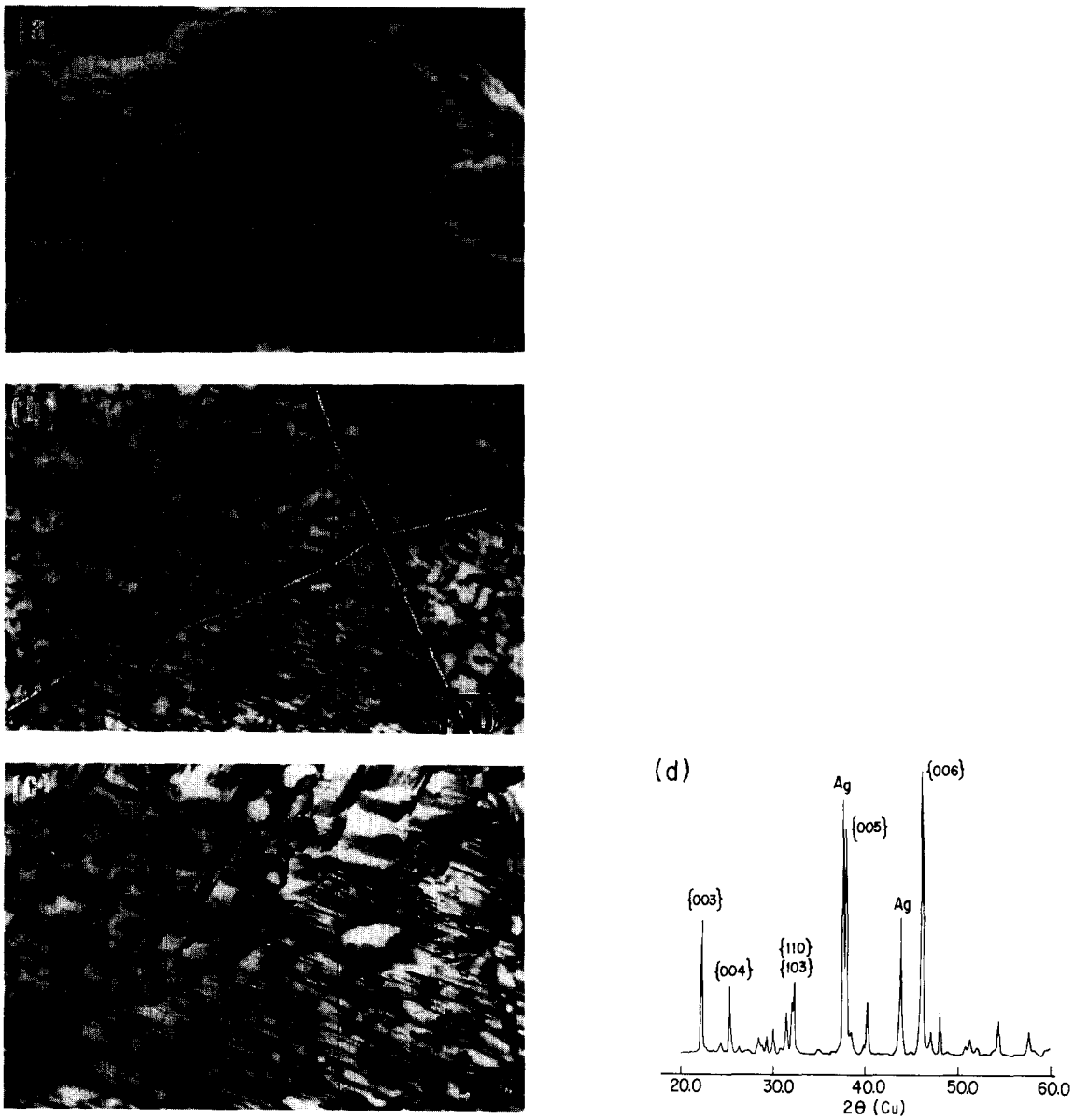

Fig. 4. Characteristics of the VMG-123-on-Ag composite tape. Shown are the morphologies of the 123 film (a) before and (b), (c) after the VMG treatment. The dashed lines in (b) trace four 123 domain boundaries. (d) The XRD pattern of the resulting 123 film, indicating texture of *c*-axis normal to the Ag substrate.

123/Ag composite. Clearly, the Ag substrate has participated the melting–resolidification reaction of the 123 film. However, since there has been no sign of melting of the Ag substrate as a whole, such a 123/Ag chemical interaction is likely to be limited over a thin layer at the interface. This interaction may, in fact, strengthen the interfacial bonding.

4. Discussion

The object of this study is to explore the possibility to lower the MG processing temperature so that MG methodology can be employed to process 123/Ag composites in different forms. Examples shown here indicate that the MG processing temperature can in-

deed be lowered, while the microstructures and superconducting properties typical of the MG-123 material can be retained by reducing the oxygen partial pressure, and further lowered by the presence of Ag. The viable solidification temperatures and oxygen pressures are found to be consistent with the solidus lines of 123 and 123/Ag reported in the literature [18,25–27]. It is noted that the solidus lines shown in Fig. 1 were originally obtained based on atmospheric experiments [18,27]. This consistency may suggest that the same low-$P(O_2)$ approach can equally successfully be carried out under a 1 atm setup with diluted oxygen. An atmospheric-pressure process (with diluted oxygen) is expected to reduce the extent of Ag loss via evaporation, while it will be more suitable for the processing of long 123/Ag tapes or wires via, for example, the zone-melting approach [30–32]. Nevertheless, working with partial vacuum facilitates the decomposition of $BaCo_3$ [33–35], which often exists in the solid-state sintered 123 preforms either due to incomplete reaction or to corrosion. Carbonate contamination is known to be detrimental to the superconductivity of 123.

As described in Section 1, one of the purposes to combine 123 oxide with Ag is for better mechanical properties. In this regard, the function of the Ag substrate in a 123-on-Ag tape is apparent; it provides the major mechanical support to the oxide film. The prerequisite for fulfilling such a function is a good interfacial bonding between 123 film and Ag substrate, which can be achieved in the PVMG process as observed in this work. For the bulk 123/Ag composite, the contribution of Ag to the mechanical properties of the composite depends heavily on the Ag distribution within the bulk, which, in turn, is determined by how Ag is dispersed in the melt and how growth fronts of 123 domains interact with the dispersed Ag phases in the melt during solidification.

As observed in the partially solidified samples which were quenched during solidification via route B, Ag exists in the melt as dispersed particles, or droplets, of which the surfaces are embedded with high densities of 211 particles (Fig. 5a). The Ag particles are mostly spherical for an Ag content less than 20 wt.%, and become more irregularly shaped as the Ag content increases. For some Ag particles located close to the growth fronts of 123 domains, they were often found to be 'bridged' with the oxide domains by 123 grains protruding from the flat growth fronts (Fig. 5b). It appears that the 123 grains near the Ag particles grow faster than the rest along the front. In other cases where Ag particles are partially engulfed into 123 domains, 123 was found to preferentially grow along the surfaces of the Ag particles (Fig. 5c). Previous kinetic studies have established that the growth of 123 in the MG process is rate-limited by the diffusion of Y from the 211 particles in the melt to the 123 growth fronts [36,37]. It is possible that the presence of the embedded 211 particles results in a higher Y concentration in the vicinity of the Ag particles, which, in turn, may have guided 123 to preferentially grow toward and finally encapsulate the Ag particles during solidification.

It is noted that, in the composites processed following route A, which employs higher processing temperatures than route B, the Ag particles in the melt do not have 211 particles embedded along their surfaces. These Ag particles were mostly not engulfed into 123 domains but trapped within the domain boundary regions (Fig. 2a). It appears that the 211-free Ag particles do not show the same 'affinity' toward the 123 domain as the 211-embedded ones and they are likely to be continuously pushed back in the melt by the growth fronts of 123 domains. How the 211 particles are trapped within the surfaces of the Ag particles during melting and how such a process is affected by temperature is currently under further investigation.

The observations of fewer and shorter cracks within the bulk 123/Ag composites as the amount of intra-domain Ag inclusions increases, as shown by the comparisons among Figs. 2a–2e, may indicate toughening of the 123 domain by Ag inclusions. Toughening of a brittle material by reinforcement with a dispersed ductile phase has drawn much attention in recent years in the field of structural ceramics [38–40]. Phenomenologically, when bonded to the brittle matrix, ductile inclusions intercepted by a crack can perform plastic deformation to absorb energy, and hereby reduce the crack driving force or the stress intensity at the crack tip. However, the extent of such improvement is known to depend not only on the ductility of the inclusion but also on the strength of matrix–inclusion interfacial bonding. A too-low interfacial bonding strength results in preferential propagation of crack along the interface. On the other

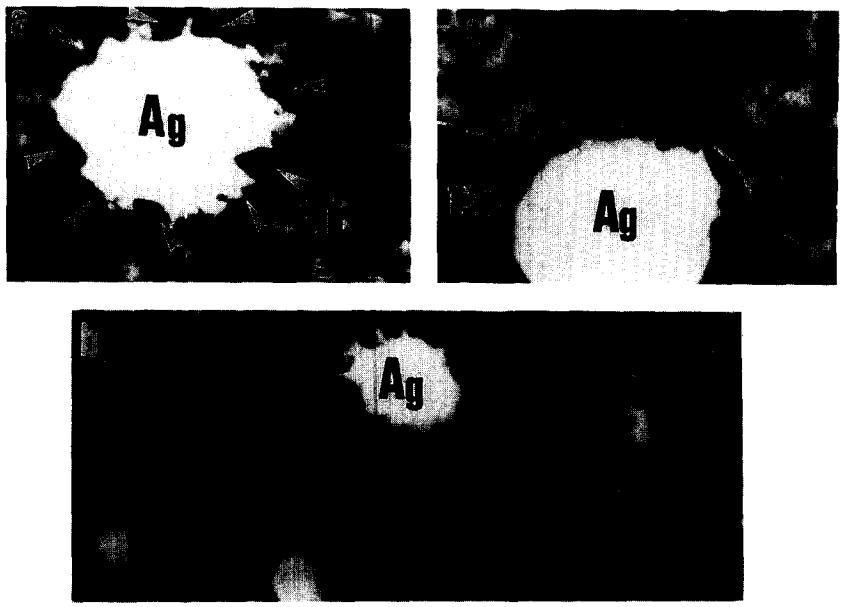

Fig. 5. The states of Ag phase during the VMG process. Shown are the Ag particles located (a) in the melt; (b) near a growth front of a 123 domain; and (c) partially engulfed in a 123 domain. The scale bars in (a) and (c) represent a length of 10 μm. The arrows in (a) indicate the embedded 211 particles within the surface layer of the Ag particle, while the dashed line in (c) delineates the growth front of 123.

hand, a too-high bonding strength does not allow the ductile inclusions to deform. In both cases, improvement is limited. Significant improvement in toughness has been predicted in the case of the intermediate interfacial bonding strength which allows a certain extent of debonding in order to remove the constraint and to allow the inclusion to neck, i.e., to stretch, as schematically shown in Fig. 6a. The salient features of such a stretching mechanism have been indeed frequently observed at the intersections between cracks and the intra-domain Ag inclusions.

For example, Fig. 6b shows an intentionally created, by mechanical means, large crack intersecting an Ag inclusion (as well as several 211 ones). Debonding between 123 and Ag occurs at the crack–Ag–123 contacts, as indicated by the white arrows in the figure. Extensive stretching of the Ag inclusion is evidenced by the formation of a 'neck' bridging the portions of Ag located at the opposite sides of the crack. It is also noticed that, along the crack, there are many 211 inclusions that are fully fractured, as indicated by the black arrows. No sign of plastic deformation of the 211 inclusion has been observed. If one assumes that these 211 and Ag particles are originally subjected to the same stress intensity due to their closeness (this may particularly be true between the Ag inclusion and the 211 one right next to it), the different extents of fracturing exhibited by these Ag and 211 inclusions may indicate that the intra-domain Ag inclusions are, in fact, able to impose a greater resistance to crack growth than the 211 ones.

The processing examples shown here only serve to demonstrate some characteristics of the PVMG process. Both the superconducting and mechanical properties of the specimens reported in this work are clearly far from being optimized. Lessons learned from the conventional MG processes can mostly be adopted for further improvement. For example, one may consider to intentionally impose a temperature gradient during solidification in order to improve the linkage and alignment among 123 domains [30–32], or to vary the cooling rate for obtaining a larger domain size, which could result in a greater magnetization. The dispersion of the 211 and Ag inclusions could also be improved with intermittent grinding as in the case of the MPMG approach.

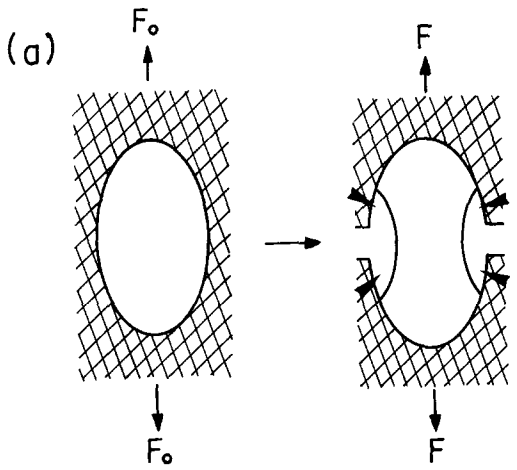

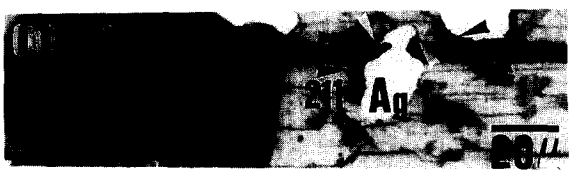

Fig. 6. (a) The schematic representation showing toughening of a brittle matrix by the stretching of a ductile inclusion. The four small arrows appearing in the diagram on the right indicate the locations of matrix–inclusion debonding. (b) Microstructure showing a crack intersecting Ag and 211 inclusions. The white arrows indicate the locations of debonding between 123 and Ag, while the black ones indicate some fully fractured 211 inclusions.

5. Summary

The methodology of melt-growth processing of 123 oxide has been extended, by reducing the processing oxygen pressure and introducing Ag, to a lower temperature regime that is suitable for the processing of the 123/Ag composite. Examples of processing 123/Ag composites in bulk and tape forms are demonstrated. While showing the superconducting and microstructural characteristics of the MG-123 material, samples thus synthesized also exhibit many properties that cannot be achieved via the current high-temperature MG processes. In this regard, the processed 123/Ag bulk composites contain uniformly distributed Ag inclusions, which are effective in reducing cracking within 123 domains. On the other hand, the 123-on-Ag tapes exhibit *c*-axis preferential orientation of the 123 film normal to the Ag substrate, good oxide–substrate adhesion, and negligible substrate melting. The engulfment of Ag inclusions into 123 domains seems to be effected by the presence of 211 particles within the surface layers of Ag particles in melt. This is not seen in the high-temperature processes.

Acknowledgements

This work is supported by the National Science Council, Republic of China under the contract number NSC 83-0405-E002-013.

References

[1] S. Jin, T. Tiefel, R. Sherwood, R. van Dover, M. Davis, G. Kammlott and R. Fastnacht, Phys. Rev. B 37 (1988) 7850.
[2] M. Murakami, M. Morita, K. Doi and K. Miyamoto, Jpn. J. Appl. Phys. 28 (1989) 1189.
[3] M. Murakami, Mod. Phys. Lett. 4 (1990) 163.
[4] M. Murakami, S. Gotoh, N. Koshizuka, S. Tanaka, T. Matsushita, S. Kanbe and K. Kitazawa, Cryogenics 30 (1990) 390.
[5] D.F. Lee, V. Selvamanickam and K. Salama, Physica C 202 (1992) 83.
[6] W.C. Wei and W.H. Lee, Jpn. J. Appl. Phys. 31 (1992) 1305.
[7] J.P. Singh, H.J. Leu, R.B. Poeppel, E. Van Voorhees, G.T. Goudey, K. Winsley and Donglu Shi, J. Appl. Phys. 66 (1989) 3154.
[8] J.P. Singh, J. Joo, D. Dingh, T. Warzynski and R.B. Poeppel, J. Mater. Res. 8 (1993) 1226.
[9] D.S. Kupperman, J.P. Singh, J. Faber Jr. and R.L. Hitterman, J. Appl. Phys. 66 (1989) 3396.
[10] B. Dwir, B. Kellett, L. Mieville and D. Pavuna, J. Appl. Phys. 69 (1991) 4433.
[11] D. Shi and K.C. Goretta, Mater. Lett. 7 (1989) 428.
[12] D. Shi, Ming Xu, J.G. Chen, A. Umezawa, S.G. Lanan, D. Miller and K.C. Goretta, Mater. Lett. 9 (1989) 1.
[13] M.L. Kullberg, M.T. Lanagan, W. Wu and R.B. Poeppel, Supercond. Sci. Technol. 4 (1991) 337.
[14] N.L. Wu, Y.K. Wang and S.H. Lin, CHEMTECH (1992) 713.
[15] P. McGinn, N. Zhu, W. Chen, M. Lanagan and U. Balachandran, Physica C 167 (1990) 343.
[16] J.A. Xia, H.T. Ren, Y. Zhao, C. Andrikidis, P.R. Munroe, H.K. Liu and S.X. Dou, Physica C 215 (1993) 152.
[17] T. Oka, Y. Itoh, Y. Yanagi, H. Tanaka, S. Takashima, Y. Yamada and U. Mizutani, Physica C 200 (1992) 55.
[18] T.B. Lindemer, F.A. Washburn, C.S. MacDougall, R. Feenstra and O.B. Cavin, Physica C 178 (1991) 93.

[19] Y. Matsuoka, E. Ban and H. Ogawa, J. Phys. D: Appl. Phys. 22 (1989) 1935.
[20] Y. Matsuoka, E. Ban, H. Ogawa and A. Suzumura, Supercond. Sci. Technol. 4 (1991) 62.
[21] A.M. Figueredo, M.J. Cima, M.C. Flemings and J.S. Haggerty, Metall. Mater. Trans. A 25A (1994) 1747.
[22] J.K.R. Weber, P.C. Nordine, K.C. Goretta and R.B. Poeppel, J. Mater. Res. 9 (1994) 1657.
[23] B.T. Ahn, V.Y. Lee and R. Beyers, Physica C 162–164 (1989) 883.
[24] T. Wada, N. Suzuki, A. Ichinose, Y. Yaegashi, H. Yamauchi and S. Tanaka, Appl. Phys. Lett. 57 (1990) 81.
[25] Y. Idemoto and K. Fueki, Jpn. J. Appl. Phys. 29 (1990) 2729.
[26] G.M. Kale, Supercond. Sci. Technol. 5 (1992) 333.
[27] T.B. Lindemer, F.A. Washburn and C.S. MacDougall, Physica C 196 (1992) 390.
[28] C.P. Bean, Phys. Rev. Lett. 8 (1962) 250.
[29] R. Feenstra, T.B. Lindemer, J.D. Budai and M.D. Galloway, J. Appl. Phys. 69 (1991) 6569.
[30] H. Wang, H. Herman, H.J. Wiesmann, Y. Zhu, Y. Xu, R.L. Sabatini and M. Suenaga, Appl. Phys. Lett. 57 (1990) 2495.
[31] P.J. McGinn, W. Chen, N. Zhu, U. Balachandran and M.T. Lanagan, Physica C 165 (1990) 480.
[32] S. Karabashev and Th. Wolf, Mater. Lett. 16 (1993) 331.
[33] G.G. Peterson, B.R. Weinberger, L. Lynds and H.A. Krasinski, J. Mater. Res. 3 (1988) 605.
[34] U. Balachandran, R.B. Poeppel, J.E. Emerson, S.A. Johnson, M.T. Lanagan, C.A. Youngdahl, D. Shi and K.C. Goretta, Mater. Lett. 8 (1989) 454.
[35] T.B. Lindemer, F.A. Washburn, C.S. MacDougall and O.B. Cavin, Physica C 174 (1991) 135.
[36] T. Izumi and Y. Shiohara, J. Mater. Res. 7 (1992) 16.
[37] T. Izumi, Y. Nakamura and Y. Shiohara, J. Mater. Res. 7 (1992) 1621.
[38] L.S. Sigl, P.A. Mataga, B.J. Dalgleish, R.M. McMeeking and A.G. Evans, Acta Metall. 36 (1988) 945.
[39] M.S. Newkirk, A.W. Urqhart and H.R. Zwicker, J. Mater. Res. 1 (1986) 81.
[40] F. Erdogan and P.F. Joseph, J. Am. Ceram. Soc. 72 (1989) 262.